

# Electronic Structure and Anion Photoelectron Spectroscopy of Uranium–Gold Clusters $\text{UAu}_n^-$ , $n = 3-7$

Rachel M. Harris,<sup>||</sup> Zhaoguo Zhu,<sup>||</sup> Burak A. Tufekci, Deepika,<sup>||</sup> Purusottam Jena,\* Kirk A. Peterson,\* and Kit H. Bowen\*



Cite This: *J. Phys. Chem. A* 2023, 127, 7186–7197



Read Online

ACCESS |



Metrics & More

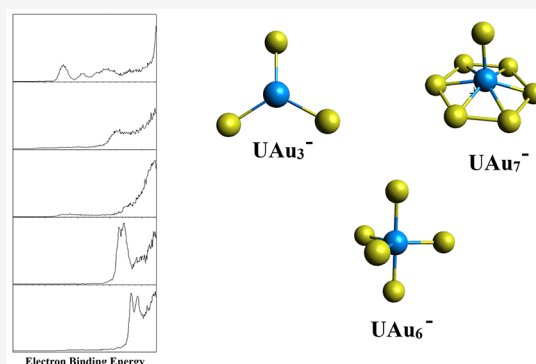


Article Recommendations



Supporting Information

**ABSTRACT:** A collaborative effort between experiment and theory toward elucidating the electronic and molecular structures of uranium–gold clusters is presented. Anion photoelectron spectra of  $\text{UAu}_n^-$  ( $n = 3-7$ ) were taken at the third (355 nm) and fourth (266 nm) harmonics of a Nd:YAG laser, as well as excimer (ArF 193 nm) photon energies, where the experimental adiabatic electron affinities and vertical detachment energies values were measured. Complementary first-principles calculations were subsequently carried out to corroborate experimentally determined electron detachment energies and to determine the geometry and electronic structure for each cluster. Except for the ring-like neutral isomer of  $\text{UAu}_6$  where one unpaired electron is spread over the Au atoms, all other neutral and anionic  $\text{UAu}_n$  clusters ( $n = 3-7$ ) were calculated to possess open-shell electrons with the unpaired electrons localized on the central U atom. The smaller clusters closely resemble the analogous  $\text{UF}_n$  species, but significant deviations are seen starting with  $\text{UAu}_5$  where a competition between U–Au and Au–Au bonding begins to become apparent. The  $\text{UAu}_6$  system appears to mark a transition where Au–Au interactions begin to dominate, where both a ring-like and two heavily distorted octahedral structures around the central U atom are calculated to be nearly isoenergetic. With  $\text{UAu}_7$ , only ring-like structures are calculated. Overall, the calculated electron detachment energies are in good agreement with the experimental values.



## INTRODUCTION

Actinide-transition metal (An-TM) bonds with a single An atom and multiple TM atoms are of fundamental interest to experimental and theoretical chemists tasked with elucidating the complicated electronic structure of such exotic complexes, especially when the TM is a coinage metal.<sup>1-6</sup> Much debate lies in describing the role that 5f electrons of An atoms play in such multifaceted structures, which often lead to a degree of covalency amongst 5f-element complexes.<sup>7</sup> The similarity in energies between 5f and 6d orbitals in the actinides and the radial extent of these orbitals (with the 6d being more diffuse) lead to a competing effect that makes interpreting the character of 5f orbitals fairly arduous.<sup>8</sup> Above all, however, the core reason for such difficulty has been attributed to relativistic effects that accompany heavy elements. Such effects are the salient reasons for the cubic structure of polonium, liquid state of mercury, and the color of gold.<sup>9,10</sup>

In addition, gold nanoclusters, both in its pure and transition metal-doped forms, have also received attention in the past few decades for their relativistic effects that can promote 5d–6s hybridization as well as a high degree of covalent bonding amongst gold atoms. TM-doped Au clusters can exhibit sigma ( $\sigma$ ) aromaticity amongst the Au atoms, bringing about stable planar structures, with species like  $\text{ZnAu}_9^-$  even displaying

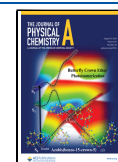
double  $\sigma$  aromaticity.<sup>11-13</sup> Furthermore, comparable relativistic effects happen to be an explanation for the high electron affinity of gold, and its electron acceptor abilities, allowing it to form ionic bonds in solid-state alkali metal auride complexes.<sup>14</sup>

However, sigma aromaticity does not always dominate when it comes to determining the structure of metal-doped gold clusters since the possibility of halogen mimicry in gold has resurfaced once again in the primarily computation-driven area of actinide–gold (An–Au) clusters. The question “When does gold behave as a halogen?” was asked years ago and still to this day left with an unsatisfactory answer, with  $\text{UAu}_4$  and  $\text{ThAu}_4$  being the systems of choice for such consideration.<sup>15</sup> This has been addressed with a recent computational work with a larger Au count in An–Au clusters, which are planar and show a high degree of sigma aromaticity and has even led to a class of clusters by the name of *Saturnenes*, for their delocalized electron ring-like orbit around the actinide atom.<sup>16,17</sup> The size-

Received: May 22, 2023

Revised: August 2, 2023

Published: August 17, 2023



dependent phenomenon, as observed in the catalytic activity in pure gold clusters, can also be a contribution toward creating a linkage between sigma aromaticity and halogen mimicry in actinide–gold nanoclusters.

Studies on smaller actinide clusters provide tremendous insights into the nature of actinide bonding.<sup>18–25</sup> However, our understanding is still limited regarding An–TM clusters.<sup>26–34</sup> Analogous to the theoretical studies investigating the similarities of actinide–platinum complexes with their actinide–oxygen analogs,<sup>35</sup> gold has been suggested as an isolobal analog to both hydrogen and the halogens, as it has the highest electron affinity of the metals and has been shown to have highly ionic character in bonding.<sup>36–38</sup> Comparison of the photoelectron spectra of  $\text{Au}_n^-$  with their analogous  $\text{Au}_{n-1}\text{H}^-$  counterparts shows noteworthy similarities, which led to the earliest notion of hydrogen-like behavior of gold.<sup>39</sup> Wang and co-workers showed that gold has halogen-like behavior in  $\text{TiAu}_4$  and hydrogen-like behavior in  $\text{Si–Au}$ .<sup>40,41</sup> Gagliardi reported that gold is halogen-like in several systems, including actinide–tetraauride systems.<sup>15,42</sup> Recently, due to similarities in the photoelectron spectra of  $\text{Au}_2\text{F}_n^-$  and  $\text{AuF}_{n+1}$  ( $n = 1$  or  $2$ ), DFT calculations have given insights into experimental evidence for the halogen-like behavior of gold.<sup>43</sup> Lately, these results have been augmented by the photoelectron spectra of  $\text{UAu}_6^-$ , where we have investigated to what extent gold could mimic fluorine and analogized it to  $\text{UF}_6^-$ .<sup>44</sup>

In the present work, we provide a synergistic study involving anion photoelectron spectroscopy (aPES) experiments together with a first-principles quantum chemistry approach based on both density functional theory (DFT) and coupled cluster calculations (CC) to investigate the electronic structure and nature of bonding of  $\text{UAu}_n$  as well as their parent anions  $\text{UAu}_n^-$  for  $n = 3–7$ . The current work provides direct evidence of the transition from predominately U–Au ionic bonding (halogen-like) to motifs with extensive Au–Au bonding.

## METHODS

**Experimental Details.** When conducting anion PES, a mass-selected negative ion beam is crossed with a fixed-frequency photon beam. The resultant photodetached electrons are directed into a magnetic bottle where they are energy-analyzed. The electron binding energy (EBE) is then determined using the energy conservation relationship:

$$\text{EBE} = h\nu - \text{EKE}$$

where EBE is the difference between the photodetached electron's kinetic energy (EKE) and the photon energy ( $h\nu$ ). Our apparatus consists of a laser vaporization cluster anion source, a time-of-flight mass spectrometer, a Nd:YAG photodetachment laser, and a magnetic bottle energy analyzer.<sup>45</sup> The magnetic bottle photoelectron spectrometer resolution is  $\sim 35$  meV at  $\text{EKE} = 1$  eV.  $\text{UAu}_n^-$  clusters were generated in our apparatus using a dual-rod laser vaporization source. Rotating, translating rods of uranium and gold were independently ablated using second harmonic (nm) photons from two Nd:YAG lasers. As each metal was vaporized, a pulse of gas consisting of 10% argon in helium ( $\sim 80$  psi) was used to induce clustering and direct the ion beam toward the extraction region. Mass spectra were obtained via time-of-flight mass spectrometry.  $\text{UAu}_n^-$  clusters of interest were mass-gated into an interaction region, where photoelectrons were detached using the third (355 nm) and fourth (266 nm) harmonic output of a Nd:YAG laser, as well as 193 nm

photons from an excimer laser. The resulting photoelectron spectra were recorded and calibrated against the well-known atomic transitions of  $\text{Cu}^-$ .<sup>46</sup>

**Computational Details.** First-principles calculations are carried out using spin-polarized density functional theory (DFT) as implemented in the Gaussian 16 program.<sup>47,48</sup> The exchange–correlation potential was treated using the Becke 3-parameter Lee–Yang–Parr (B3LYP) hybrid functional along with a correlation consistent polarized valence double- $\zeta$  (cc-pVDZ-PP) basis set for both U and Au atoms.<sup>49–52</sup> The empirical dispersion corrections to the DFT energies were included using a Grimme's D3 damping function.<sup>53</sup> The relativistic effect of the core electrons in the U and Au atoms was incorporated using the 60-electron Stuttgart/Cologne energy-consistent effective core pseudopotentials (ECP60MDF).<sup>54,55</sup> Quadratic convergence algorithms were used during the optimization process without any symmetry constraint. For each cluster, the optimized ground state geometries of the neutral and anionic  $\text{UAu}_n$  ( $n = 3–7$ ) clusters were obtained by comparing the lowest singlet, triplet, and quintet states for even electron systems and doublets, quartets, and sextets for odd electron systems. These calculations included multiple isomers. We also compared DFT results with restricted open-shell CCSD(T) with the MOLPRO program<sup>56,57</sup> using both cc-pVDZ-PP and cc-pVTZ-PP basis sets for  $\text{UAu}_6$ , and the results were in good agreement.<sup>44</sup> In the latter calculations, all valence electrons were correlated except for the 6s electrons of U. For other clusters, we have only used DFT results. The calculated adiabatic detachment energy (ADE) of the anion or analogously the electron affinity (EA) of the neutral is defined in this work as the equilibrium value and is the energy difference between the anion and its corresponding neutral, both at their respective ground state equilibrium geometries, whereas the vertical detachment energy (VDE) is the energy difference between the anion and its corresponding neutral, both at the ground state equilibrium geometry of the anion. The terms ADE and EA will be used interchangeably throughout this text. The optimized geometry of each cluster was confirmed to be a true minimum by ensuring that all the vibrational frequencies were real. The electronic structure and bonding were analyzed using the natural bond order (NBO) analysis (v.7.0),<sup>58</sup> the Mayer bond order (MBO),<sup>59</sup> and the Laplacian of the electron density ( $\nabla^2\rho(r)$ ). The adaptive natural density partitioning (AdNDP) analysis was performed using the Multiwfn package.<sup>60</sup>

## RESULTS AND DISCUSSION

The resulting mass spectrum of the U/Au system is displayed in Figure 1. Pure gold clusters ( $\text{Au}_2^-$ – $\text{Au}_{17}^-$ ) were observed and are marked in the figure with red stars. A smaller peak 41 amu following each  $n + 1$  gold cluster ( $\text{Au}_{n+1}^-$ ) peak was identified to be  $\text{UAu}_n^-$  (where  $n = 3–16$ ) and are indicated by blue hash marks in Figure 1. Because an argon gas mixture was used as a backing gas, the possibility of argon-tagged gold clusters was addressed.<sup>61,62</sup> Argon tagging would create a mass peak 40 amu greater than its parent gold cluster, and the overlap of these argon-tagged gold cluster peaks with the uranium–gold cluster peaks could convolute the PES of the  $\text{UAu}_n^-$  clusters. To reveal the presence of argon tagging, mass spectra were taken without the presence of uranium by simply refraining from ablating the uranium rod. Secondary argon-tagged gold cluster peaks were not observed.

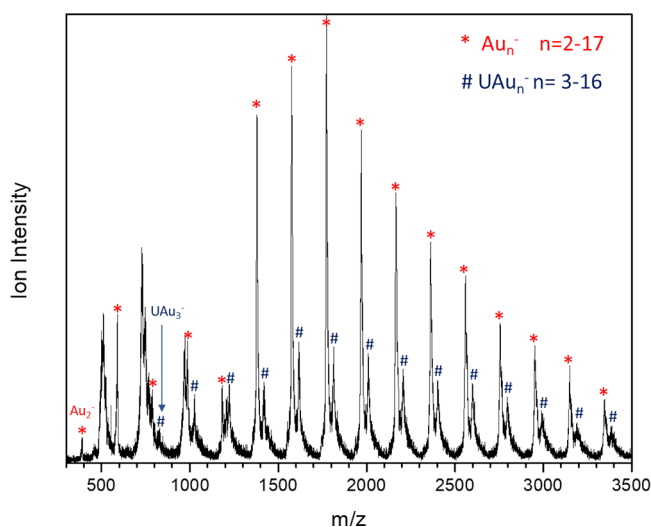


**Figure 1.** Mass spectrum resulting from laser vaporization of Au and U rods, pulsed with a 10% Ar in He gas mixture. Gold clusters are marked with a red star, starting with  $Au_2^-$ . The peaks observed 41 amu after a gold cluster peak, labeled with blue hash marks, are  $UAu_n^-$  peaks, starting with  $UAu_3^-$ . Other peaks located in the low mass region are uranium oxides.

The photoelectron spectra of  $UAu_n^-$  ( $n = 3-7$ ) taken with 3.49, 4.66, and 6.42 eV photons are displayed in Figure 2. The PES of other  $UAu_n^-$  clusters ( $n = 8-13$ ) are available in the SI as Figures S1, S2, and S3. The first feature in the  $UAu_3^-$  spectra appears with an onset at 1.28 eV, with a maximum value at 1.56 eV. A second broad feature begins at  $\sim 4.4$  eV and spans to  $\sim 5.0$  eV. This is presumably due to the excited electronic states of the neutral. The spectra of  $UAu_4^-$  reveal a broad band that begins around 2.60 eV and reaches a peak value at 3.20 eV. Two more dominant peaks, at 4.92 and 5.13 eV, are revealed at our highest photon energy. The  $UAu_5^-$  spectrum exhibits a very broad feature beginning at  $\sim 1.3$  eV, peaking at 3.48 eV. Due to the broad nature of this initial onset, it is suspected that fragmentation of  $UAu_5^-$  occurs. Using Gaussian regression as a guide, the true onset of the first peak is then estimated to be closer to 3.2 eV. A higher EBE peak at 3.64 eV is also observed. The first peak observed in the  $UAu_6^-$  spectrum has an onset around 3.05 eV with a peak value observed at 3.28 eV, and a second, broader feature is observed around 3.2–3.3 eV. The  $UAu_7^-$  spectrum has its initial peak starting around 2.56 eV with a peak value observed at 3.67 eV. A second major peak is observed at 3.88 eV. As an approximation, the adiabatic detachment energy (ADE) is estimated to be the EBE at  $\sim 10\%$  of the rising photoelectron intensity.<sup>63</sup> In addition, the vertical detachment energy (VDE) is determined as the EBE value of the fitted intensity maximum in the lowest EBE peak. Error bars of  $\pm 0.1$  eV have been assigned to the VDE values based on the estimated uncertainties of the fits to the maxima of the origin peaks. The ADEs are estimates and as such do not have error bars ascribed to them.

The first step of our theoretical approach is to identify the ground state geometries and low-lying isomers of the neutral and anionic  $UAu_n$  ( $n = 3-7$ ) clusters. The DFT optimized energy values of neutral and anionic  $UAu_n$  ( $n = 3-7$ ) along with the corresponding spin multiplicities are provided in Table S1 of the SI. A variety of techniques as outlined in the previous section were used to study the nature of bonding and

the electronic structure at their ground state geometries. The electron affinities (EA) and vertical detachment energies (VDE) are calculated from the total energies of the neutral and anionic clusters and compared with the corresponding experimental values. Good agreement between theory and experiment gives confidence in the validity of the calculated geometries and electronic properties.

**Equilibrium Geometries and Ground Electronic States of Neutral and Anionic Clusters.** We begin our discussions with the electronic ground states and DFT optimized geometries of neutral and anionic  $UAu_n$  clusters ( $n = 3-7$ ), as shown in Table 1 and Figure 3.

$UAu_3$ ,  $UAu_3^-$ . Both neutral and anionic  $UAu_3$  have  $C_{3v}$  symmetry with U–Au bond lengths of 2.79 and 2.93 Å, respectively. The ground state spin multiplicities are quartet and quintet for the neutral and anion, respectively. The corresponding unpaired electrons occupy three U 5f orbitals for the neutral and three U 5f and one U 7s6d mixed orbital for anionic  $UAu_3$ . Hence, these species are very analogous to the electronic ground states of both  $UF_3$  and  $UF_3^-$  where the lowest energy electron detachment arises from primarily a 7s orbital on U.<sup>64</sup>

$UAu_4$ ,  $UAu_4^-$ . The geometries of both neutral and anionic  $UAu_4$  are distorted with a symmetry lower than  $T_d$  symmetry, tending more toward  $D_{2d}$ . The U–Au bond lengths in neutral and anionic  $UAu_4$  are about 2.71 and 2.88 Å, respectively. The open-shell orbitals contributing toward the spin multiplicity are two U 5f for the neutral and three U 5f for the anionic  $UAu_4$  clusters. Correspondingly, the ground state spin multiplicities are triplet and quartet, respectively. These are also consistent with previous DFT calculations for  $UF_4/UF_4^-$ , although when spin–orbit coupling was included, the ground state of  $UF_4^-$  was determined to have a  $5f^2 7s^1$  ground state configuration.

$UAu_5$ ,  $UAu_5^-$ . The geometry of neutral  $UAu_5$ , unlike those of the  $UAu_3$  and  $UAu_4$  clusters, is significantly different from its anion, with the latter having  $D_{3h}$  symmetry. During the optimization of neutral  $UAu_5$ , the three Au atoms (i.e., Au1, Au2, and Au3) initially placed in the same plane as in its anion (with  $D_{3h}$  symmetry) move toward each other, while the other two Au atoms (i.e., Au4 and Au5) initially placed out of plane also move toward each other, thus lowering the symmetry of neutral  $UAu_5$ , as shown in Figure 3. This is the first instance where a  $UAu_n$  cluster exhibits significant Au–Au bonding, and  $UAu_5$  resembles the interaction of a Au trimer with a  $UAu_2$  cluster. The neutral and anionic  $UAu_5$  clusters prefer quartet and triplet spin states, respectively, and the corresponding open-shell orbitals are three U 5f and two U 5f, respectively. The latter is analogous to  $UF_5^-$  or  $UCl_5^-$ , but the equilibrium structure and ground electronic state of neutral  $UAu_5$  differ significantly from those of  $UX_5$  ( $X = F$  and  $Cl$ ),<sup>65</sup> which has  $C_{4v}$  symmetry and a  $5f^1$  open-shell doublet configuration. The  $5f^3$  configuration of  $UAu_5$  can be rationalized as the interaction of an open-shell doublet  $Au_3$  fragment<sup>66</sup> with the  $5f^3 7s^1$  configuration of  $UAu_2$  (assuming the same electron configuration of  $UF_2$ ). The equilibrium geometry of  $UF_5^-$  was also previously calculated at the DFT level of theory to have  $C_{4v}$  symmetry, unlike  $D_{3h}$  for  $UAu_5^-$  as found in this work.<sup>64</sup> For both  $UF_5$  and  $UF_5^-$  however, higher order correlation and spin–orbit effects were reported to stabilize the  $D_{3h}$  structure,<sup>52</sup> which was low-lying even at the scalar relativistic level.

$UAu_6$ ,  $UAu_6^-$ . In the case of neutral and anionic  $UAu_6$ , three nearly isoenergetic isomers are observed, as shown in Figure 3.

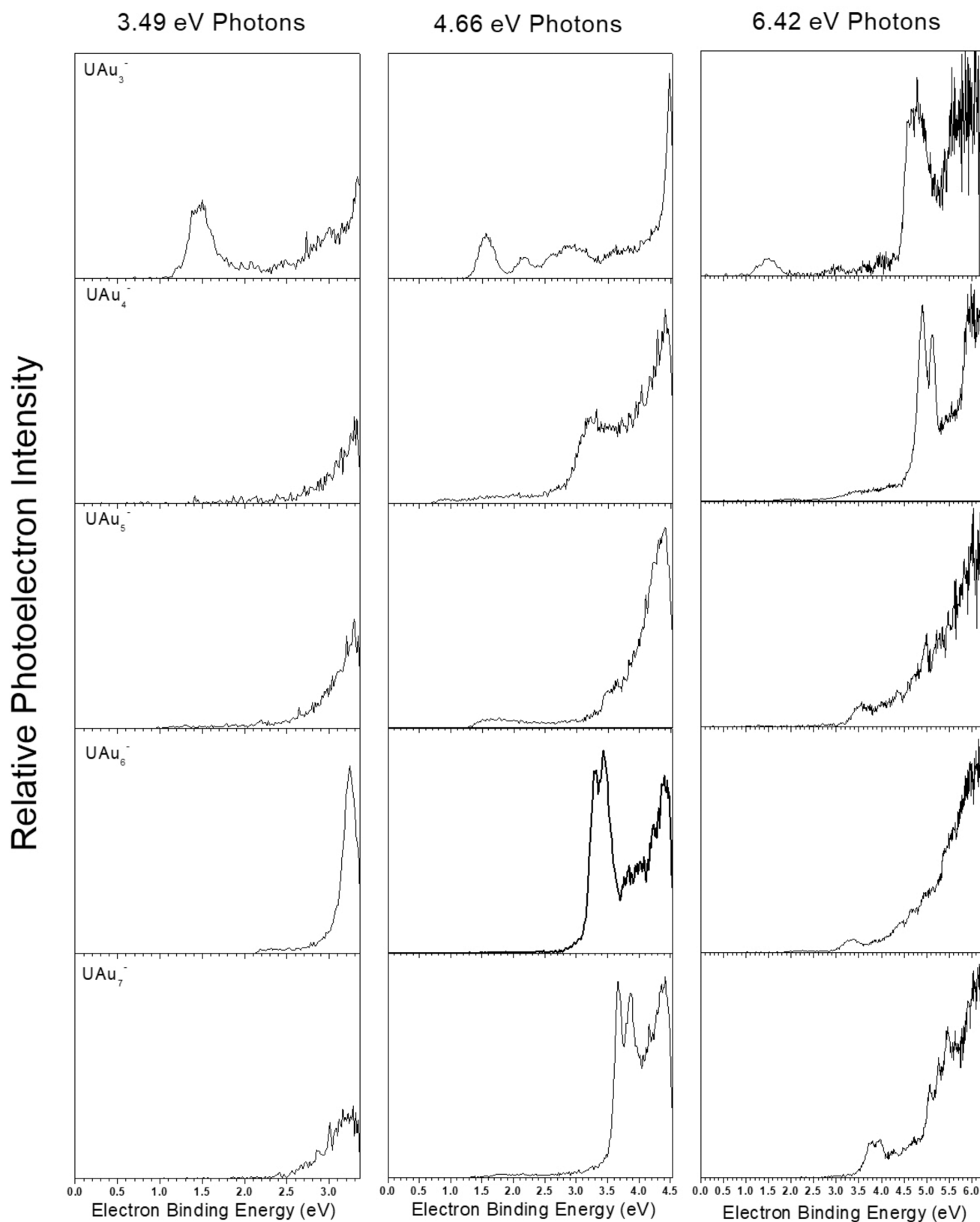


**Figure 2.** Photoelectron spectra of  $\text{UAu}_n^-$  ( $n = 3-7$ ) taken with the third (3.49 eV) and fourth harmonics (4.66 eV) of a Nd:YAG photodetachment laser, as well as an excimer (6.42 eV) photodetachment laser.

We categorize the three isomers of  $\text{UAu}_6^-$  as (1) a ring-type (Isomer I), where the six Au atoms are arranged in a ring with the U atom at its center, (2) a quasi-octahedral (Isomer II), where four of the Au atoms form a rectangular configuration,

while the other two are located on opposite sides of U, and (3) a butterfly-type geometry (Isomer III), where the U atom lies on a plane with four of the six Au atoms. The U–Au bond lengths in the neutral and anionic  $\text{UAu}_6$  clusters range from

Table 1. Calculated DFT Electronic Structure Properties of Neutral and Anionic  $UAu_n$  Clusters ( $n = 3-7$ )<sup>a</sup>

system	symmetry	bond lengths (Å)		$q(U)$	$q(Au)$
		U–Au	Au–Au		
<sup>4</sup> UAu <sub>3</sub>	$C_{3v}$	2.79	4.64	1.43	−0.48
<sup>3</sup> UAu <sub>4</sub>	$D_{2d}$	2.71	4.30	1.34	−0.32/−0.35
<sup>4</sup> UAu <sub>5</sub>	$C_1$	2.79	2.61/3.64	1.16	−0.05/−0.42
<sup>5</sup> UAu <sub>6</sub> (I)	$C_1$	3.02	2.74	0.71	−0.01/−0.21
<sup>3</sup> UAu <sub>6</sub> (II)	$C_1$	2.86	2.83	0.77	−0.01/−0.26
<sup>3</sup> UAu <sub>6</sub> (III)	$C_1$	2.87	2.72	0.80	+0.02/−0.27
<sup>4</sup> UAu <sub>7</sub>	$C_s$	3.11	2.70	0.50	−0.07
<sup>5</sup> UAu <sub>3</sub> <sup>−</sup>	$C_{3v}$	2.93	5.07	0.90	−0.63
<sup>4</sup> UAu <sub>4</sub> <sup>−</sup>	$D_{2d}$	2.88	4.70	1.32	−0.58
<sup>3</sup> UAu <sub>5</sub> <sup>−</sup>	$D_{3h}$	2.77	3.91	1.08	−0.39/−0.43
<sup>4</sup> UAu <sub>6</sub> <sup>−</sup> (I)	$C_1$	2.97	2.85	0.40	−0.23
<sup>4</sup> UAu <sub>6</sub> <sup>−</sup> (II)	$C_1$	3.00	2.82	0.83	−0.15/−0.48
<sup>4</sup> UAu <sub>6</sub> <sup>−</sup> (III)	$C_1$	3.02	2.72	0.88	−0.09/−0.51
<sup>3</sup> UAu <sub>7</sub> <sup>−</sup>	$C_1$	2.90/2.74	2.82	0.02	0.10/−0.37

<sup>a</sup>The leftmost superscripts on the molecular formulas indicate the spin multiplicity, the bond lengths correspond to average values, and the atomic charges (min/max on Au) are from the NPA analysis.

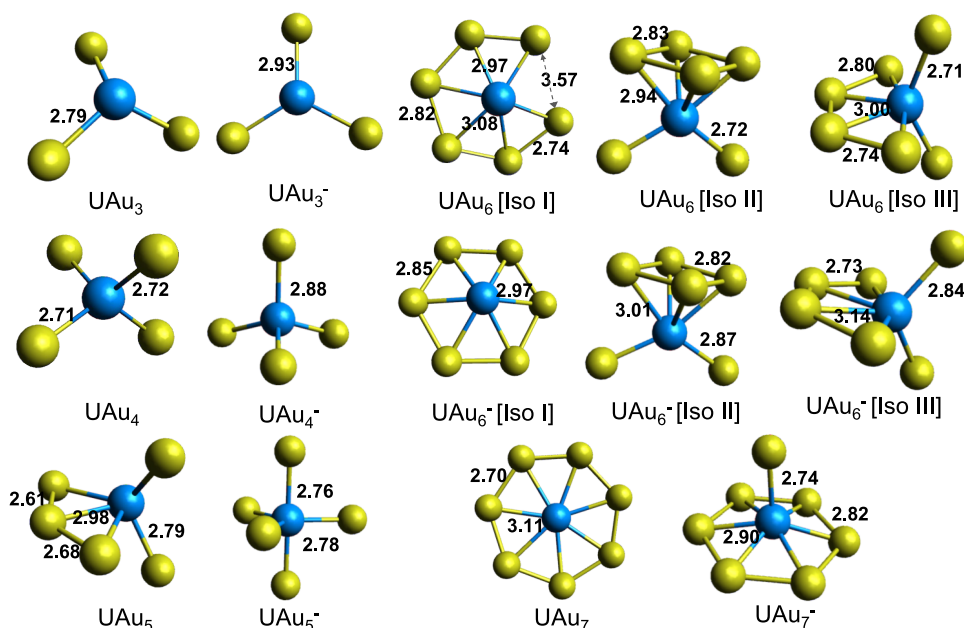


**Figure 3.** Optimized ground state geometries of neutral and anionic  $[UAu_n]$  ( $n = 3-7$ ) at the B3LYP-D3/cc-pVDZ-PP level of theory. Blue and metallic green spheres represent the U and Au atoms, respectively. The bond lengths of the U–Au and Au–Au bonds in Å are provided along the bonds.

2.97 to 3.00 Å and from 2.78 to 3.14 Å, respectively. The preferred spin multiplicities for Isomer I of the neutral and anion of  $UAu_6$  are quintet and quartet, respectively, whereas for Isomers II and III, they are triplets and quartets, respectively. The open-shell electrons contributing toward the spin-multiplicities reside in U 5f orbitals in all cases, except for Isomer I of the neutral where one unpaired electron is spread over the Au atoms. All three isomers involve significant Au–Au interactions, particularly in the case of Isomer I. Isomers II and III can be considered either strongly distorted octahedrons by analogy with the structure of  $UF_6$  or alternatively the interaction of small Au clusters with  $UAu_n$  fragments. For both Isomers II and III, the structures are hence the result of a competition between U–Au and Au–Au

bonding. Comprehensive discussion of the relative energetics of all three isomers of the neutral and anionic  $UAu_6$  clusters was provided in our previous paper.<sup>44</sup> At the CCSD(T)/cc-pVTZ-PP level of theory using the DFT optimized geometries, Isomer III is calculated to be the ground state of the neutral (both Isomers I and II are higher in energy by about 0.4 eV), while Isomer I is the lowest energy for the anion with Isomer III being higher in energy by just 0.22 eV and Isomer II by 0.53 eV. Hence, both Isomers I and III are expected to be represented in the PES and perhaps Isomer II as well.

$UAu_7$ ,  $UAu_7^-$ . The optimized geometry of neutral  $UAu_7$  is closely related to the ring-like (Isomer I) geometry of  $UAu_6$  without any buckling pattern. Here, Au atoms form a planar ring around the central U atom, whereas for anionic  $UAu_7$ , one

Au atom moves to the top of the central U atom, as shown in Figure 3. The U–Au bond lengths in neutral and anionic  $\text{UAu}_7$  are 3.11 and 2.90 (2.74) Å, respectively (see Figure 3). During the optimization of  $\text{UAu}_7^-$ , the migration of one Au atom to the top of the U atom is mostly caused by the dominating U–Au interactions over Au–Au repulsions. The preferred spin-multiplicities of neutral and anionic  $\text{UAu}_7$  clusters are quartet and triplet, respectively, and the corresponding unpaired electrons occupy three U 5f orbitals for the neutral and two U 5f orbitals for anionic  $\text{UAu}_7$ .

**Electron Affinities and Vertical Detachment Energies.** In Table 2, the calculated electron affinities (EA) and vertical

**Table 2. Experimental and Calculated Adiabatic Detachment Energies (ADE) and Vertical Detachment Energies (VDE) for  $\text{UAu}_n^-$  ( $n = 3-7$ ) Clusters<sup>a</sup>**

species	ADE (eV)		VDE (eV)	
	exp.	theory	exp.	theory
$\text{UAu}_3^-$	1.28	1.45	$1.56 \pm 0.1$	1.61
$\text{UAu}_4^-$	2.60	2.96	$3.20 \pm 0.1$	3.39
$\text{UAu}_5^-$	3.20	2.87	$3.48 \pm 0.1$	3.84
$\text{UAu}_6^-$	3.05	2.99/3.04/3.07* (3.15/2.59/2.62)	$3.28 \pm 0.1$	3.18/3.34/3.40* (3.34/3.12/3.16)
$\text{UAu}_7^-$	2.56	2.72	$3.67 \pm 0.1$	3.59

<sup>a</sup>The DFT calculated values for  $\text{UAu}_6^-$  are provided for its three isomers in the order of IsomI/IsomII/IsomIII. CCSD(T)/cc-pVTZ-PP values calculated at the DFT geometries are given in parentheses.

detachment energies (VDE) of these clusters are compared with the corresponding results obtained from the photoelectron spectra using the 4.66 eV photon energy. The calculated ADE and VDE of  $\text{UAu}_3^-$  are 1.45 and 1.61 eV, respectively, and agree well with the corresponding experimental values of 1.28 and 1.56 eV. The analogous values for  $\text{UAu}_4^-$ , namely, 2.96 and 3.39 eV, respectively, are also in reasonably good agreement with the experimental values of 2.60 and 3.20 eV, particularly for the VDE. The calculated ADE and VDE for  $\text{UAu}_5^-$  are 2.87 and 3.84 eV, respectively. The large difference between the EA and VDE for  $\text{UAu}_5$

reflects the significant difference in the geometries of the neutral and anionic clusters, which is consistent with the broad peak in the PES of  $\text{UAu}_5^-$ . The initial onset at 1.3 eV observed in the PES of  $\text{UAu}_5^-$  reflects in situ fragmentation of  $\text{UAu}_5$  into small  $\text{UAu}_3$  and  $\text{Au}_2$  clusters. To confirm the in situ fragmentation of  $\text{UAu}_5$  into  $\text{UAu}_3$  and  $\text{Au}_2$  with the first/second photon interactions, the change in energy ( $\Delta E$ ) required for the fragmentation of anionic and neutral  $\text{UAu}_5$  was calculated at the DFT level of theory using the expressions

$$\Delta E_1(\text{UAu}_5^-) = E(\text{UAu}_3^-) + E(\text{Au}_2) - E(\text{UAu}_5^-)$$

$$\Delta E_2(\text{UAu}_5) = E(\text{UAu}_3) + E(\text{Au}_2) - E(\text{UAu}_5)$$

The calculated  $\Delta E_1$  and  $\Delta E_2$  values are 3.59 and 2.17 eV for the fragmentation of anionic and neutral  $\text{UAu}_5$ , respectively. In both cases, the energy required for the fragmentation is less than the energy of the second photon (4.66 eV). Therefore, the first broad peak observed in the PES of  $\text{UAu}_5^-$  represents the electron detachment from  $\text{UAu}_3^-$ , thus the EA of  $\text{UAu}_3$ . This is further evidenced by the low intensity and broadening of the first peak in the PES of  $\text{UAu}_5^-$ . The calculated VDE and EA of 3.84 and 2.87 eV for  $\text{UAu}_5^-$  and  $\text{UAu}_5$ , respectively, are consistent with the experimental VDE and EA of 3.48 and 3.2 eV, respectively.

For  $\text{UAu}_6^-$ , the calculated VDE and ADE of 3.18 and 2.99 eV, respectively, of Isomer I agree well with the experimental values of 3.28 and 3.05 eV, respectively (Table 2). Not surprisingly, the calculated EA and VDE values of Isomers II and III are also close to the experimental values. The VDE values calculated at the CCSD(T)/cc-pVTZ-PP level of theory as reported in our previous study<sup>44</sup> differ slightly from the DFT results, with values ranging from 3.16 to 3.34 eV (the DZ values were about 0.1 eV smaller than those with TZ). These isomers are found to be nearly isoenergetic with very similar VDE values. Thus, all three isomers could be present in the spectrum shown in Figure 2, but particularly Isomers I and III. Considering the steep rise in the first peak in the PES of  $\text{UAu}_6^-$ , the EA and VDE must be closely related. In the case of  $\text{UAu}_7$ , the experimental EA and VDE of 2.56 and 3.67 eV are

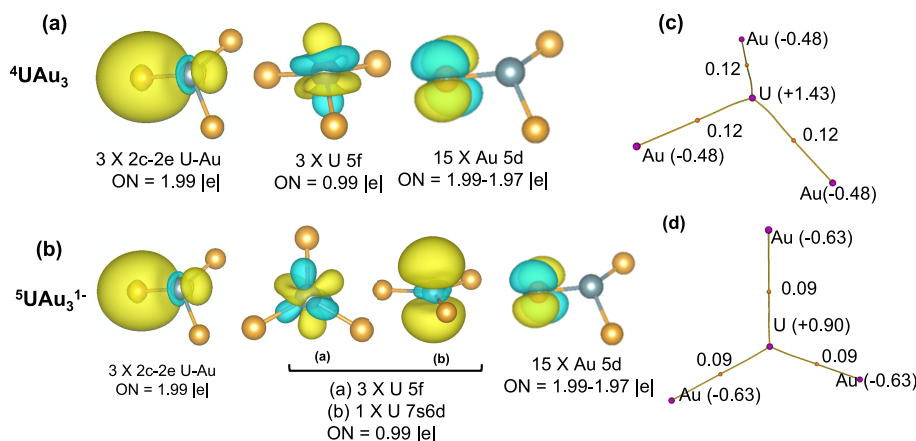


**Figure 4.** Electronic structure and bonding analysis of neutral and anionic  $\text{UAu}_3$  clusters. Adaptive natural density partitioning (AdNDP) analysis of (a) neutral  $\text{UAu}_3$  and (b)  $\text{UAu}_3^-$ . Bader's quantum theory of atoms in molecule (QTAIM) topology of (c) neutral  $\text{UAu}_3$  and (d)  $\text{UAu}_3^-$ . The pink and orange dots represent the atom-centered and bond-centered critical points (BCP). The numbers at the BCP are the corresponding Laplacian electron density ( $\nabla^2\rho(r)$ ) values (in the atomic units). The NPA charges (in units of e) are provided in the parentheses along with the atom symbols. Yellow and blue colors in AdNDP analysis represent the charge accumulation and depletion regions, respectively. Orange and gray spheres represent the Au and U atoms, respectively. Superscripts in the U atom represent the spin multiplicity of the cluster.

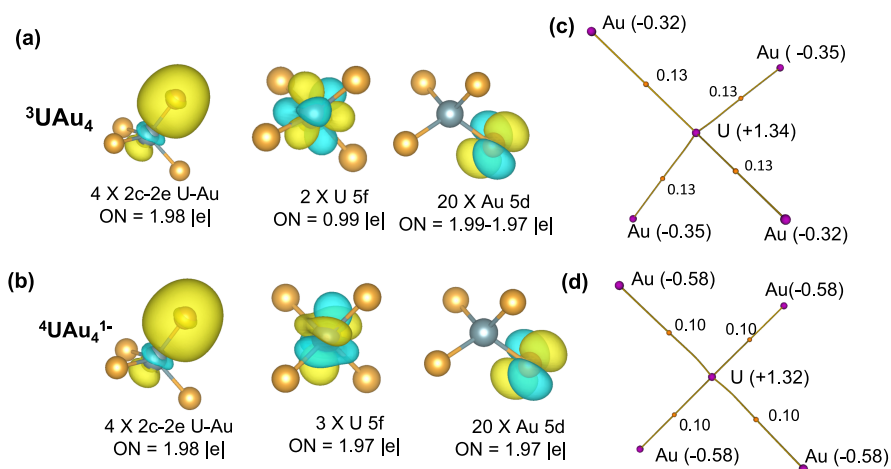


**Figure 5.** Electronic structure and bonding analysis of  $UAu_4$  clusters. AdNDP analysis of (a) neutral  $UAu_4$  and (b)  $UAu_4^-$ . QTAIM topologies of (c) neutral  $UAu_4$  and (d)  $UAu_4^-$ . The pink and orange dots represent the atom-centered and bond-centered critical points (BCP). The number at the BCP are the corresponding  $\nabla^2\rho(r)$  values (in the atomic units). The NPA charges (in units of e) are provided in the parentheses along with the atom symbols. Yellow and blue colors in AdNDP represent the charge accumulation and depletion regions, respectively. Orange and gray spheres represent the Au and U atoms, respectively.

again consistent with the calculated EA and VDE of 2.72 and 3.59 eV, respectively.

**Nature of Bonding and Electronic Structure of Neutral and Anionic Clusters.** The nature of bonding and the electronic structure of the clusters of this study were studied using the calculated NPA charges on the atoms, the adaptive natural density partitioning (AdNDP) analysis, and Bader's quantum theory of atom in molecules (QTAIM) analysis. In the following, we discuss these properties for  $UAu_n$  ( $n = 3-7$ ) clusters.

$UAu_3$ ,  $UAu_3^-$ . For  $UAu_3$ , the NPA charges on U and Au atoms are +1.43 and  $-0.48e$ , respectively (see Table 1 and Figure 4c,d). In  $UAu_3^-$ , the corresponding charges on U and Au atoms are +0.90 and  $-0.63e$ , respectively. While the additional electron in the anion occupies a U 5f orbital, it only partially reduces the charge on U and the bonds are more strongly polarized toward the Au atoms in the anion. The U–Au bond orders obtained from the MBO analysis are 1.22 and 1.13 in the neutral and anionic clusters, respectively, indicative of a strong sigma bond between U and each Au atom. The smaller MBO values in  $UAu_3^-$  are consistent with the longer U–Au bond.

The nature of bonding in  $UAu_3$  and  $UAu_3^-$  is further analyzed using the AdNDP method. The results are shown in Figure 4a,b. The occupation number (ON) represents the number of electrons participating in the bond formation, with a maximum value of  $2|e|$  per bond. In  $UAu_3$ , U possesses three unpaired electrons in 5f orbitals with ON values of 0.99|e|, which corresponds to three singly occupied Lewis lone pairs. Each of the three Au atoms in  $UAu_3$  contains five doubly occupied (5d) orbitals, thus contributing a total of 15 (5d)-orbitals. The corresponding ONs of Au are 1.99|e| in each case. In addition, three two-center two-electron pairs (2c-2e) of  $UAu_3$  participate in the formation of three U–Au ionic bonds with about 80% being contributed by Au and 20% by U. In the case of  $UAu_3^-$ , U possesses four unpaired electrons where three come from its 5f orbitals and one from hybrid orbital consisting of 7s (67%) and 6d (33%) with an ON of 0.99|e|. The three 2c-2e pairs with ONs of 1.99|e| forming three U–Au bonds in  $UAu_3^-$  have ionic character with nearly 81% coming from Au and 19% from U.

The nature of bonding is further confirmed using the Bader's quantum theory of atom in molecules (QTAIM) analysis. The topologies of the neutral and anionic  $UAu_3$  clusters using the QTAIM analysis are shown in Figure 4c,d, respectively. The bond critical points (BCP) between two atoms within a molecule confirm the existence of a chemical bond, and the sign of the values of Laplacian of electron density ( $\nabla^2\rho(r)$ ) at the BCP defines the nature of interaction between the corresponding atoms. A negative value of the Laplacian of electron density ( $\nabla^2\rho(r) < 0$ ) at the BCP implies a covalent nature of the bond, while a positive value indicates a noncovalent (ionic/polar) nature. The positive values of  $\nabla^2\rho(r)$  at the BCPs, namely, 0.12 and 0.09 au in neutral and anionic  $UAu_3$ , respectively, further confirm the ionic nature of the bonds.

$UAu_4$ ,  $UAu_4^-$ . The NPA charges on the U and Au atoms in  $UAu_4$  are +1.34e and  $-0.32$  ( $-0.35$ )e, respectively, where two Au atoms carry  $-0.32e$ , while the other two carry  $-0.35e$  (Figure 5c). In  $UAu_4^-$ , on the other hand, the NPA charges on the U and Au atoms are +1.32 and  $-0.58e$ , respectively. Hence, while the additional electron in the anion resides in a localized U 5f orbital, the charge distribution is even more strongly polarized toward the Au atoms than in the neutral. The MBO bond orders of the U–Au bonds are 1.34 and 1.06, confirming the strong sigma bonds between the U and Au atoms, with a relatively stronger bond in the neutral than in the anionic  $UAu_4$  cluster.

The results of the AdNDP analysis are shown in Figure 5a,b. In  $UAu_4$ , U carries two unpaired electrons occupying its 5f orbitals, which correspond to two singly occupied Lewis lone pairs with ON values of 0.99|e|. Each of the four Au atoms in neutral  $UAu_4$  contributes five doubly occupied 5d orbitals, creating five Lewis lone pairs with ON values of 1.97–1.99|e| (see Figure 5a). Along with this, four two-center two-electron pairs (2c-2e) participate in the formation of four U–Au ionic bonds in  $UAu_4$  with 71% contribution coming from Au and 29% from U. In  $UAu_4^-$ , U has three unpaired electrons coming from its three singly occupied 5f orbitals, which correspond to three Lewis lone pairs (see Figure 5b). In addition, four U–Au bonds formed due to 2c-2e pairs with ON values of 1.98|e| in

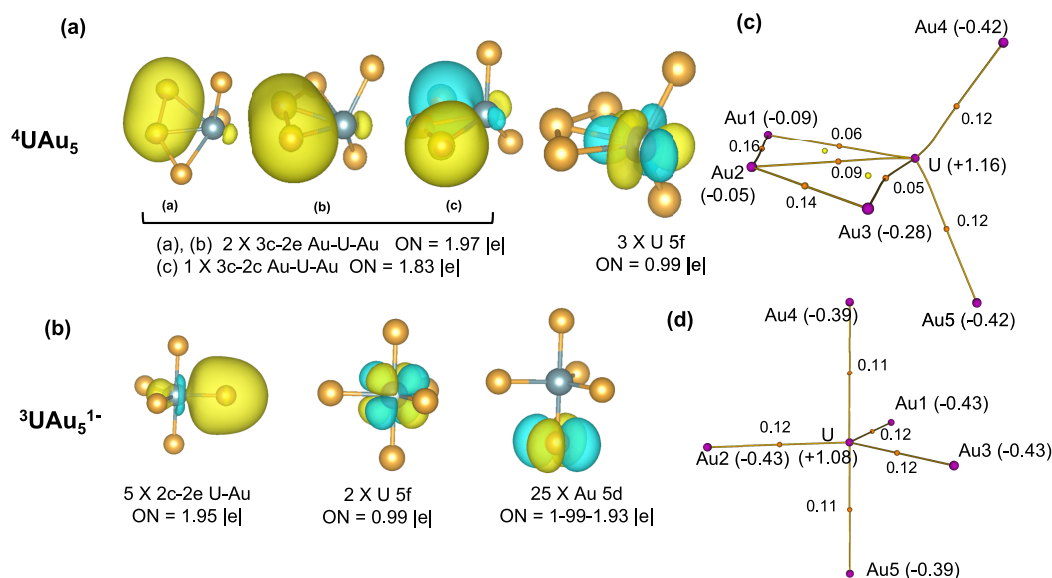


**Figure 6.** Electronic structure and bonding analysis of  $UAu_5$  clusters. AdNDP analysis of (a) neutral  $UAu_5$  and (b)  $UAu_5^{1-}$ . QTAIM topology of (c) neutral  $UAu_5$  and (d)  $UAu_5^{1-}$ . The pink and orange dots represent the atom-centered and bond-centered critical points (BCP). The number at the BCP are the corresponding  $\nabla^2\rho(r)$  values (in the atomic units). The NPA charges (in units of  $e$ ) are provided in the parentheses along with the atom symbols. Yellow and blue colors in AdNDP represent the charge accumulation and depletion regions, respectively. Orange and gray spheres represent the Au and U atoms, respectively.

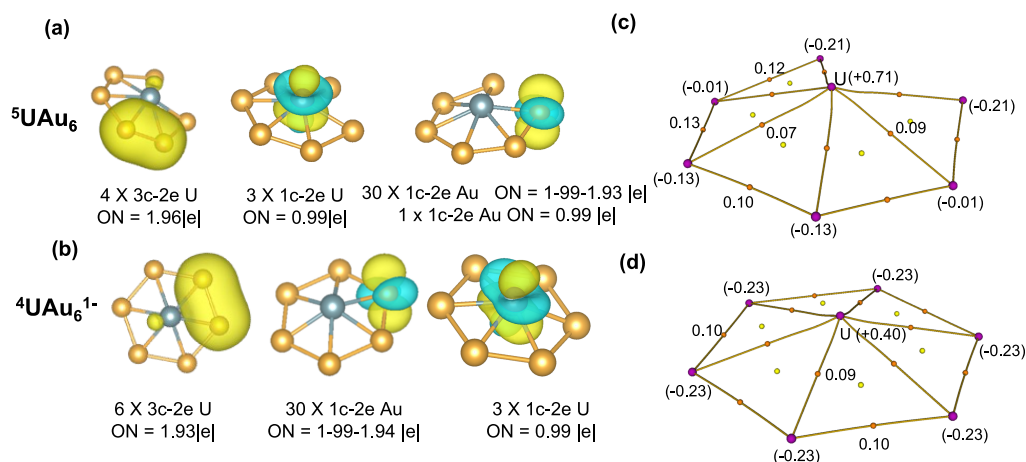


**Figure 7.** Electronic structure and bonding analysis of  $UAu_6$  clusters (IsomI). AdNDP analysis of (a) neutral  $UAu_6$  and (b)  $UAu_6^{1-}$ . Bader's QTAIM topology of (c) neutral  $UAu_6$  and (d)  $UAu_6^{1-}$ . The pink and orange dots represent the atom-centered and bond-centered critical points (BCP). The number at the BCP are the corresponding  $\nabla^2\rho(r)$  values. Yellow and blue colors in AdNDP represent the charge accumulation and depletion regions, respectively. Orange and gray spheres represent the Au and U atoms, respectively.

$UAu_4^{1-}$  are ionic in character with 76% contributed by Au and 24% by U.

To verify further the ionic nature of U–Au bonding in  $UAu_4$  clusters, Bader's QTAIM analysis is performed; the topologies for neutral and anionic  $UAu_4$  are shown in Figure 5c,d, respectively. The positive values of  $\nabla^2\rho(r)$  at the BCPs, 0.13 and 0.10 au for neutral and anionic  $UAu_4$ , respectively, are consistent with the ionic nature of the bonds.

$UAu_5$ ,  $UAu_5^{1-}$ . The NPA charge on U in  $UAu_5$  is +1.16e, while those on Au range from  $-0.42$  to  $-0.05e$  (see Figure 6c). The very small charges on two of the Au atoms in the plane with U suggest the interaction of a Au dimer with a distorted  $UAu_3$  fragment. This is consistent with the lower oxidation state on the U atom with its concomitant higher number of open-shell 5f electrons (three) compared to the symmetric  $U(V)F_5$  cluster, which only has one unpaired 5f

electron. In the highly symmetric  $UAu_5^{1-}$  cluster, U carries a charge of +1.08e, while Au carries charges ranging from  $-0.43e$  for the equatorial atoms to  $-0.39e$  for the axial atoms.

The bond orders of U–Au bonds computed using the MBO analysis in  $UAu_5$  range between 0.39 and 0.56 for the three Au atoms (i.e., U–Au1, U–Au2, and U–Au3) and 1.19 for the other two Au atoms (i.e., U–Au4 and U–Au5). This implies that all the Au atoms bind strongly with U. However, Au4 and Au5 have a stronger bond strength than Au1, Au2, and Au3 with the U atom. The MBO bond order for U–Au in  $UAu_5^{1-}$  is 1.20 for the axial bonds and 1.23 for those in the equatorial plane. This shows nearly the same strength of all the U–Au bonds in the  $UAu_5^{1-}$  cluster, which is again consistent with the high symmetry of the  $UAu_5^{1-}$  cluster.

The results of the AdNDP analysis revealing the nature of bonding in the  $UAu_5$  clusters are shown in Figure 6a,b. In

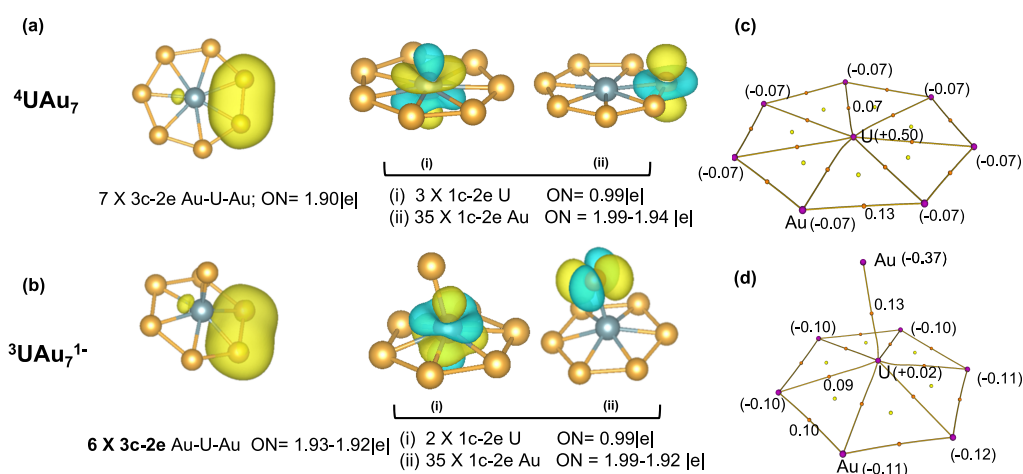


**Figure 8.** Electronic structure and bonding analysis of UAu<sub>7</sub> clusters. AdNDP analysis of (a) neutral UAu<sub>7</sub> and (b) UAu<sub>7</sub><sup>-</sup>. Bader's QTAIM topology of (c) neutral UAu<sub>6</sub> and (d) UAu<sub>5</sub><sup>-</sup>. The pink and orange dots represent the atom-centered and bond-centered critical points (BCP). The number at the BCP are the corresponding Laplacian electron density ( $\nabla^2\rho(r)$ ) values. Yellow and blue colors in AdNDP represent the charge accumulation and depletion regions, respectively. Orange and gray spheres represent the Au and U atoms, respectively.

UAu<sub>5</sub>, the U atom carries three unpaired electrons in its 5f orbitals, which implies that U has three singly occupied Lewis lone pairs with ON values of 0.99|e|. Along with this, in UAu<sub>5</sub>, three Au atoms placed nearly in the same plane (i.e., Au1, Au2, and Au3) participate in the formation of two small rings using three-center two-electron (3c-2e) bond configurations with ON values of 1.97|e| and one ring using 3c-2e bond with an ON value of 1.83|e|, as shown in Figure 6a. In UAu<sub>5</sub>, all the five U–Au bonds are ionic in nature formed using a 2c-2e pair with ON values of 1.95|e| with 69% contributed by Au and 31% by U. The U atom carries two unpaired electrons coming from two singly occupied U 5f orbitals, which correspond to two Lewis lone pairs with ON values of 0.99|e| (see Figure 6b). To verify further the ionic nature of U–Au bonding in UAu<sub>5</sub> clusters, Bader's QTAIM analysis is performed, and the topologies for neutral and anionic UAu<sub>5</sub> clusters are examined as shown in Figure 6c,d, respectively. The positive values of  $\nabla^2\rho(r)$  at BCP further confirm the ionic nature of the U–Au bond in the UAu<sub>5</sub> clusters.

**Isomer 1 of UAu<sub>6</sub> UAu<sub>6</sub><sup>-</sup>.** The NPA charge on U in UAu<sub>6</sub> (Isom1) is +0.71e, while those on Au around the ring range from -0.21 to -0.01e (see Figure 7c). As shown in Figure 7d, in UAu<sub>6</sub><sup>-</sup>, each of the six Au atoms carries an NPA charge of -0.23e, while U has a charge of +0.40e. In the formation of the anion, the added electron spin pairs with the open-shell electron distributed amongst the Au atoms in the neutral, resulting in just three unpaired 5f electrons on U.

For the UAu<sub>6</sub> cluster, U participates in the formation of four 3c-2e pairs forming four U-(Au)<sub>2</sub> bonds with ON values of nearly 1.96|e|, as shown in Figure 7a,b. (The Au-Au pair opposite the open Au-Au linkage is the pair not involved in a 3c-2e bond.) The formation of 2c-2e bonds between U and Au includes about 78% contribution by Au and 22% by U, and thus U–Au bonds are ionic in nature. In addition, UAu<sub>6</sub> possesses four unpaired electrons, where amongst these, three electrons come from U 5f orbitals and the fourth unpaired electron is distributed over the Au atoms, which corresponds to four singly occupied Lewis lone pairs. In the case of UAu<sub>6</sub><sup>-</sup>, the addition of an electron makes the ring geometry more symmetric. Thus, instead of four, we have six 3c-2e bonds with ON values of 1.93|e| and six 2c-2e pairs with ON 1.99|e|, with

71% contribution coming from Au and 29% from U. Therefore, bonding between U and Au in the UAu<sub>6</sub> clusters is again ionic in nature. The U–Au bond orders obtained from the MBO analysis vary in the range of 0.55–0.77 for the neutral and 0.71–0.72 for the anionic clusters, which indicates strong sigma bonds between U and each Au atom in UAu<sub>6</sub> clusters. The numerous 3c-2e bonds in these ring structures demonstrate the increased importance of Au–Au metallic bonding in these larger clusters.

The electronic structure and nature of bonding are further confirmed using Bader's QTAIM, as shown in Figure 7c,d. For both neutral and anionic UAu<sub>6</sub>, the positive values of the Laplacian of electron density, ( $\nabla^2\rho(r)$ ) about 0.09e at BCP between U and Au, but also about 0.10e between the Au atoms, further confirm the ionic nature of the bonding in UAu<sub>6</sub> clusters.

**UAu<sub>7</sub>, UAu<sub>7</sub><sup>-</sup>.** For UAu<sub>7</sub>, the NPA charges on U and each of the seven Au atoms are +0.50 and -0.07e, respectively (see Figure 8c). Here, each of the seven Au atoms carry the same charge, which reflects the higher symmetry of the planar ring-like geometry of UAu<sub>7</sub>. Meanwhile, for the anion of UAu<sub>7</sub> (Figure 8d), the NPA charge on U is nearly zero and six of the Au atoms carry charges in the range of -0.10 to -0.12e. The seventh Au atom, which is placed at the top of the U atom, carries a -0.37e charge.

The nature of bonding in UAu<sub>7</sub> clusters is analyzed using the AdNDP technique, as shown in the Figure 8a,b. In the case of UAu<sub>7</sub>, the U atom participates in the formation of seven U-(Au)<sub>2</sub> bonds with ON values of 1.90|e| and has three unpaired electrons in its 5f orbitals. This implies that U has three singly occupied Lewis lone pairs with ON values of 0.99|e|. Along with this, each of the seven Au atoms in UAu<sub>7</sub> carries five doubly occupied (1c-2e) 5d orbitals with ON values of 1.99 to 1.94|e|. In the case of UAu<sub>7</sub><sup>-</sup>, U possesses two unpaired electrons coming from its 5f orbitals with an ON of 0.99|e|. In addition, due to the migration of one Au atom to the top of the U atom in UAu<sub>7</sub><sup>-</sup>, instead of seven, there are six U-(Au)<sub>2</sub> bonds formed with ON values in the range of 1.93–1.92|e|. In addition, the formation of 2c-2e bonds between U and Au with about 64% contribution from Au and 36% from U atoms shows that the bonding between U and Au in the UAu<sub>7</sub> cluster

is ionic in nature. In addition, the MBO bond orders between the U–Au bonds vary in the range of 0.50–0.51 for  $\text{UAu}_7$ , whereas for the anion, the MBO bond order for the six U–Au bonds forming a ring pattern varies in the range of 0.71–0.76. For the Au atom placed at the top of U atom, the corresponding U–Au bond order is about 1.25. This indicates strong sigma bonding between U and Au atoms in anionic  $\text{UAu}_7$  clusters compared to the neutral  $\text{UAu}_7$  cluster. As in Isomer I of  $\text{UAu}_6$ , the numerous 3c-2e bonds reflect the strong importance of Au–Au interactions in these larger clusters.

To verify further the ionic nature of U–Au bonding in  $\text{UAu}_7$  clusters, Bader's QTAIM analysis is performed, as shown in Figure 8c,d, respectively. The positive values of  $\nabla^2\rho(r)$  at BCP for neutral and anionic  $\text{UAu}_7$  clusters further confirm the ionic nature of U–Au bonds.

## CONCLUSIONS

By combining anion photodetachment spectroscopy with primarily DFT calculations, the present work has shown how uranium–gold clusters ( $\text{UAu}_n$ ) transition from predominately U–Au ionic bonding where Au behaves like a halogen for  $n < 5$  to a dominant role of Au–Au bonding for  $n \geq 6$ . The competition between U–Au and Au–Au interactions is well exemplified in neutral  $\text{UAu}_5$ , which contains two 3c-2e bonds, but particularly  $\text{UAu}_6$  and  $\text{UAu}_6^-$ , which involve low-lying isomers displaying varying degrees of Au–Au bonding. The low-lying ring-like isomer, which maximizes Au–Au interactions, first appears in neutral and anionic  $\text{UAu}_6$  and is the only structural motif calculated to be stable for neutral and anionic  $\text{UAu}_7$ .

## ASSOCIATED CONTENT

### Data Availability Statement

All data are available in the main text or the supplementary materials. All reasonable requests for materials will be fulfilled.

### Supporting Information

The Supporting Information is available free of charge at <https://pubs.acs.org/doi/10.1021/acs.jpca.3c03452>.

Figures S1 to S3: PES of  $\text{UAu}_n^-$  ( $n = 8–13$ ) clusters; Table S1: optimized energy values of neutral and anions of  $\text{UAu}_n$  ( $n = 3–7$ ); Cartesian coordinates and spin states of neutral and anionic  $\text{UAu}_n$  (PDF)

## AUTHOR INFORMATION

### Corresponding Authors

**Purusottam Jena** – Department of Physics, Virginia Commonwealth University, Richmond, Virginia 23284, United States; [orcid.org/0000-0002-2316-859X](https://orcid.org/0000-0002-2316-859X); Email: [pjena@vcu.edu](mailto:pjena@vcu.edu)

**Kirk A. Peterson** – Department of Chemistry, Washington State University, Pullman, Washington 99164, United States; [orcid.org/0000-0003-4901-3235](https://orcid.org/0000-0003-4901-3235); Email: [kipeters@wsu.edu](mailto:kipeters@wsu.edu)

**Kit H. Bowen** – Department of Chemistry, Johns Hopkins University, Baltimore, Maryland 21218, United States; [orcid.org/0000-0002-2858-6352](https://orcid.org/0000-0002-2858-6352); Email: [kbowen@jhu.edu](mailto:kbowen@jhu.edu)

### Authors

**Rachel M. Harris** – Department of Chemistry, Johns Hopkins University, Baltimore, Maryland 21218, United States; [orcid.org/0000-0002-3585-5258](https://orcid.org/0000-0002-3585-5258)

**Zhaoguo Zhu** – Department of Chemistry, Johns Hopkins University, Baltimore, Maryland 21218, United States; [orcid.org/0000-0002-4395-9102](https://orcid.org/0000-0002-4395-9102)

**Burak A. Tufekci** – Department of Chemistry, Johns Hopkins University, Baltimore, Maryland 21218, United States

**Deepika** – Department of Physics, Virginia Commonwealth University, Richmond, Virginia 23284, United States

Complete contact information is available at: <https://pubs.acs.org/10.1021/acs.jpca.3c03452>

### Author Contributions

<sup>||</sup>R.M.H., Z.Z., and D. made equal contributions. R.M.H., Z.Z., and B.A.T. completed the experimental photoelectron study. D., P.J., and K.A.P. performed the theoretical study. K.H.B., P.J., and K.A.P. conceived and supervised the work.

### Notes

The authors declare no competing financial interest.

## ACKNOWLEDGMENTS

K.H.B. and K.A.P. gratefully acknowledge the support of the U.S. Department of Energy (DOE), Office of Science, Office of Basic Energy Sciences, Heavy Element Chemistry program, Grant Nos. DE-SC0022977 (K.H.B.) and DE-SC0008501 (K.A.P.). P.J. acknowledges partial support from the U.S. Department of Energy, Office of Basic Energy Sciences, Division of Materials Sciences and Engineering under Award No. DE-FG02-96ER45579. Resources of the National Energy Research Scientific Computing Center supported by the Office of Science of the U.S. Department of Energy under Contract No. DE-AC02-05CH11231 is also acknowledged.

## REFERENCES

- (1) Zhang, P.; Liu, H.; Zou, W.; Zhang, P.; Hu, S.-X. Relativistic Effects Stabilize the Planar Wheel-like Structure of Actinide-Doped Gold Clusters:  $\text{An@Au}_7$  ( $\text{An} = \text{Th to Cm}$ ). *J. Phys. Chem. A* **2020**, *124*, 8173–8183.
- (2) Gao, Y.; Wang, Z. Effects of 5f-Elements on Electronic Structures and Spectroscopic Properties of Gold Superatom Model. *Chin. Phys. B* **2016**, *25*, No. 083102.
- (3) Wang, J.; Xie, W.; Wang, J.; Gao, Y.; Lei, J.; Zhang, R.-Q.; Wang, Z. Actinide Embedded Nearly Planar Gold Superatoms: Structural Properties and Applications in Surface-Enhanced Raman Scattering (SERS). *Phys. Chem. Chem. Phys.* **2018**, *20*, 27523–27527.
- (4) Gao, Y.; Dai, X.; Kang, S.; Jimenez-Cruz, C. A.; Xin, M.; Meng, Y.; Han, J.; Wang, Z.; Zhou, R. Structural and Electronic Properties of Uranium-Encapsulated Au<sub>14</sub> Cage. *Sci. Rep.* **2014**, *4*, 5862.
- (5) Gao, Y.; Chen, L.; Dai, X.; Song, R.; Wang, B.; Wang, Z. A Strong Charge-Transfer Effect in Surface-Enhanced Raman Scattering Induced by Valence Electrons of Actinide Elements. *RSC Adv.* **2015**, *5*, 32198–32204.
- (6) Wu, X.; Gao, Y.; Xie, W.; Wang, Z. Bonding Properties of a Superatom System with High-Z Elements: Insights from Energy Decomposition Analysis. *RSC Adv.* **2020**, *10*, 14482–14486.
- (7) Kaltsoyannis, N. Does Covalency Increase or Decrease across the Actinide Series? Implications for Minor Actinide Partitioning. *Inorg. Chem.* **2013**, *52*, 3407–3413.
- (8) Neidig, M. L.; Clark, D. L.; Martin, R. L. Covalency in F-Element Complexes. *Coord. Chem. Rev.* **2013**, *257*, 394–406.
- (9) Pyykkö, P. Relativistic Effects in Structural Chemistry. *Chem. Rev.* **1988**, *88*, 563–594.
- (10) Pyykkö, P. Relativistic Effects in Chemistry: More Common Than You Thought. *Annu. Rev. Phys. Chem.* **2012**, *63*, 45–64.
- (11) Tanaka, H.; Neukermans, S.; Janssens, E.; Silverans, R. E.; Lievens, P.  $\sigma$  Aromaticity of the Bimetallic  $\text{Au}_2\text{Zn}^+$  Cluster. *J. Am. Chem. Soc.* **2003**, *125*, 2862–2863.

- (12) Lin, L.; Hölzl, T.; Gruene, P.; Claes, P.; Meijer, G.; Fielicke, A.; Lievens, P.; Nguyen, M. T. Fluxionality and  $\sigma$ -Aromaticity in Small Yttrium-Doped Gold Clusters. *ChemPhysChem* **2008**, *9*, 2471–2474.
- (13) Kulichenko, M.; Chen, W.-J.; Zhang, Y.-Y.; Xu, C.-Q.; Li, J.; Wang, L.-S. Double  $\sigma$ -Aromaticity in a Planar Zinc-Doped Gold Cluster: Au<sub>9</sub>Zn. *J. Phys. Chem. A* **2021**, *125*, 4606–4613.
- (14) Pyykkö, P. Theoretical Chemistry of Gold. *Angew. Chem. Int. Ed.* **2004**, *43*, 4412–4456.
- (15) Gagliardi, L. When Does Gold Behave as a Halogen? Predicted Uranium Tetraauride and Other MAu<sub>4</sub> Tetrahedral Species, (M = Ti, Zr, Hf, Th). *J. Am. Chem. Soc.* **2003**, *125*, 7504–7505.
- (16) Pyykkö, P.; Taubert, S. Saturnenes Like Th@Au<sub>6</sub> D<sub>6h</sub>: Ring-Current Evidence for Au–Au Bonding Along the Gold Ring. *Isr. J. Chem.* **2022**, *62*, No. e202100139.
- (17) Cheng, A.; Wang, J.; Zhang, Q.; Zhu, Y.; Wang, Z. Intramolecular Bonding Properties in Actinide Embedded Nearly Planar Superatoms. *Chem. Phys. Lett.* **2020**, *752*, No. 137574.
- (18) Marshall, M.; Zhu, Z.; Harris, R.; Bowen, K. H.; Wang, W.; Wang, J.; Gong, C.; Zhang, X. ThH<sub>5</sub>: An Actinide-Containing Superhalogen Molecule. *ChemPhysChem* **2021**, *22*, 5–8.
- (19) Czekner, J.; Lopez, G. V.; Wang, L.-S. High Resolution Photoelectron Imaging of UO(–) and UO<sub>2</sub>(–) and the Low-Lying Electronic States and Vibrational Frequencies of UO and UO<sub>2</sub>. *J. Chem. Phys.* **2014**, *141*, 244302.
- (20) Li, W.-L.; Su, J.; Jian, T.; Lopez, G. V.; Hu, H.-S.; Cao, G.-J.; Li, J.; Wang, L.-S. Strong Electron Correlation in UO<sub>2</sub>–: A Photoelectron Spectroscopy and Relativistic Quantum Chemistry Study. *J. Chem. Phys.* **2014**, *140*, No. 094306.
- (21) Su, J.; Li, W.-L.; Lopez, G. V.; Jian, T.; Cao, G.-J.; Li, W.-L.; Schwarz, W. H. E.; Wang, L.-S.; Li, J. Probing the Electronic Structure and Chemical Bonding of Mono-Uranium Oxides with Different Oxidation States: UO<sub>x</sub>– and UO<sub>x</sub> (x = 3–5). *J. Phys. Chem. A* **2016**, *120*, 1084–1096.
- (22) Liu, G.; Zhang, C.; Ciborowski, S. M.; Asthana, A.; Cheng, L.; Bowen, K. H. Mapping the Electronic Structure of the Uranium(VI) Dinitride Molecule, UN<sub>2</sub>. *J. Phys. Chem. A* **2020**, *124*, 6486–6492.
- (23) Vasiliu, M.; Peterson, K. A.; Marshall, M.; Zhu, Z.; Tufekci, B. A.; Bowen, K. H.; Dixon, D. A. Interaction of Th with H<sub>0</sub>/–/+ : Combined Experimental and Theoretical Thermodynamic Properties. *J. Phys. Chem. A* **2022**, *126*, 198–210.
- (24) Marshall, M.; Zhu, Z.; Liu, J.; Cheng, L.; Bowen, K. H. Photoelectron Spectroscopic and Ab Initio Computational Studies of the Anion, HThO. *J. Phys. Chem. A* **2021**, *125*, 1903–1909.
- (25) Marshall, M.; Zhu, Z.; Liu, J.; Bowen, K. H.; Cheng, L. Anion Photoelectron Spectroscopic and Relativistic Coupled-Cluster Studies of Uranyl Dichloride Anion, UO<sub>2</sub>Cl<sub>2</sub>–. *J. Mol. Spectrosc.* **2021**, *379*, No. 111496.
- (26) Ritchey, J. M.; Zozulin, A. J.; Wroblewski, D. A.; Ryan, R. R.; Wasserman, H. J.; Moody, D. C.; Paine, R. T. An Organothorium-Nickel Phosphido Complex with a Short Thorium-Nickel Distance. The Structure of Th(η<sup>5</sup>-C<sub>5</sub>Me<sub>5</sub>)<sub>2</sub>(μ<sub>2</sub>-PPh<sub>2</sub>)<sub>2</sub>Ni(CO)<sub>2</sub>. *J. Am. Chem. Soc.* **1985**, *107*, 501–503.
- (27) Hay, P. J.; Ryan, R. R.; Salazar, K. V.; Wroblewski, D. A.; Sattelberger, A. P. Synthesis and X-ray Structure of (C<sub>5</sub>Me<sub>5</sub>)<sub>2</sub>Th(μ<sub>2</sub>-PPh<sub>2</sub>)<sub>2</sub>Pt(PMe<sub>3</sub>): A Complex with a Thorium-Platinum Bond. *J. Am. Chem. Soc.* **1986**, *108*, 313–315.
- (28) Sternal, R. S.; Brock, C. P.; Marks, T. J. Metal-Metal Bonds Involving Actinides. Synthesis and Characterization of a Complex Having an Unsupported Actinide to Transition Metal Bond. *J. Am. Chem. Soc.* **1985**, *107*, 8270–8272.
- (29) Sternal, R. S.; Sabat, M.; Marks, T. J. Metal-Metal Bonds Involving Actinides Functionalization of Activated Carbon-Hydrogen Bonds and Unusual Oligomerization Chemistry Mediated by a Thorium-Ruthenium Complex. *J. Am. Chem. Soc.* **1987**, *109*, 7920–7921.
- (30) Sternal, R. S.; Marks, T. J. Actinide-to-Transition Metal Bonds. Synthesis, Characterization, and Properties of Metal-Metal Bonded Systems Having the Tris(Cyclopentadienyl)Actinide Fragment. *Organometallics* **1987**, *6*, 2621–2623.
- (31) Gardner, B. M.; McMaster, J.; Lewis, W.; Liddle, S. T. Synthesis and Structure of [{N(CH<sub>2</sub>CH<sub>2</sub>NSiMe<sub>3</sub>)<sub>3</sub>}URE(HS-C<sub>5</sub>SH<sub>5</sub>)<sub>2</sub>]: A Heterobimetallic Complex with an Unsupported Uranium–Rhenium Bond. *Chem. Commun.* **2009**, *20*, 2851–2853.
- (32) Chi, C.; Wang, J.-Q.; Qu, H.; Li, W.-L.; Meng, L.; Luo, M.; Li, J.; Zhou, M. Preparation and Characterization of Uranium–Iron Triple-Bonded UFe(CO)<sub>3</sub>– and OUF<sub>e</sub>(CO)<sub>3</sub>– Complexes. *Angew. Chem. Int. Ed.* **2017**, *56*, 6932–6936.
- (33) Zhu, Z.; Marshall, M.; Harris, R. M.; Bowen, K. H.; Vasiliu, M.; Dixon, D. A. Th<sub>2</sub>O–, Th<sub>2</sub>Au–, and Th<sub>2</sub>AuO<sub>1,2</sub>– Anions: Photoelectron Spectroscopic and Computational Characterization of Energetics and Bonding. *J. Phys. Chem. A* **2021**, *125*, 258–271.
- (34) Zhu, Z.; Marshall, M.; Bowen, K. H.; Peterson, K. A. ThAu<sub>2</sub>–, ThAu<sub>2</sub>O–, and ThAuOH– anions: Photoelectron Spectroscopic and Theoretical Characterization. *J. Chem. Phys.* **2022**, *156*, No. 054305.
- (35) Feng, R.; Glendening, E. D.; Peterson, K. A. Coupled Cluster Studies of Platinum–Actinide Interactions. Thermochemistry of PtAnO<sup>n+</sup> (n = 0–2 and An = U, Np, Pu). *J. Phys. Chem. A* **2021**, *125*, 5335–5345.
- (36) Jung, J.; Kim, H.; Kim, J. C.; Park, M. H.; Han, Y.-K. Gold Behaves as Hydrogen in the Intermolecular Self-Interaction of Metal Aurides MAu<sub>4</sub> (M = Ti, Zr, and Hf). *Chem. – Asian J.* **2011**, *6*, 868–872.
- (37) Pyykkö, P. Theoretical Chemistry of Gold. II. *Inorg. Chim. Acta* **2005**, *358*, 4113–4130.
- (38) Erdogdu, Y.; Jian, T.; Lopez, G. V.; Li, W.-L.; Wang, L.-S. On the Electronic Structure and Chemical Bonding of Titanium Tetraauride: TiAu<sub>4</sub> and TiAu<sub>4</sub>–. *Chem. Phys. Lett.* **2014**, *610–611*, 23–28.
- (39) Buckart, S.; Ganteför, G.; Kim, Y. D.; Jena, P. Anomalous Behavior of Atomic Hydrogen Interacting with Gold Clusters. *J. Am. Chem. Soc.* **2003**, *125*, 14205–14209.
- (40) Li, X.; Kiran, B.; Wang, L.-S. Gold as Hydrogen. An Experimental and Theoretical Study of the Structures and Bonding in Disilicon Gold Clusters Si<sub>2</sub>Au<sub>n</sub>– and Si<sub>2</sub>Au<sub>n</sub> (n = 2 and 4) and Comparisons to Si<sub>2</sub>H<sub>2</sub> and Si<sub>2</sub>H<sub>4</sub>. *J. Phys. Chem. A* **2005**, *109*, 4366–4374.
- (41) Kiran, B.; Li, X.; Zhai, H.-J.; Cui, L.-F.; Wang, L.-S. [SiAu<sub>4</sub>]: Aurosilane. *Angew. Chem. Int. Ed.* **2004**, *43*, 2125–2129.
- (42) Gagliardi, L.; Pyykkö, P. Study of the MAu<sub>6</sub> (M = Cr, Mo, W) Molecular Species: A Transition from Halogenlike to Hydrogenlike Chemical Behavior for Gold. *Phys. Chem. Chem. Phys.* **2004**, *6*, 2904–2906.
- (43) Shah, A.; Banjade, H.; Long, Z.-C.; Gao, Z.-O.; Xu, H.-G.; Zheng, W.; Jena, P. Signature of Au as a Halogen. *J. Phys. Chem. Lett.* **2022**, *13*, 4721–4728.
- (44) Harris, R. M.; Zhu, Z.; Deepika; Tufekci, B. A.; Peterson, K.; Jena, P.; Bowen, K. H. Au as a Surrogate for F: The Case of UAu<sub>6</sub> vs UF<sub>6</sub>. *J. Am. Chem. Soc.* **2022**, *144*, 19685–19688.
- (45) Gerhards, M.; Thomas, O. C.; Nilles, J. M.; Zheng, W.-J.; Bowen, K. H. J. Cobalt–Benzene Cluster Anions: Mass Spectrometry and Negative Ion Photoelectron Spectroscopy. *J. Chem. Phys.* **2002**, *116*, 10247–10252.
- (46) Ho, J.; Ervin, K. M.; Lineberger, W. C. Photoelectron Spectroscopy of Metal Cluster Anions: Cu–n, Ag–n, and Au–n. *J. Chem. Phys.* **1990**, *93*, 6987–7002.
- (47) Kresse, G.; Furthmüller, J. Efficient Iterative Schemes for Ab Initio Total-Energy Calculations Using a Plane-Wave Basis Set. *Phys. Rev. B* **1996**, *54*, 11169–11186.
- (48) Frisch, M. J.; Trucks, G. W.; Schlegel, H. B.; Scuseria, G. E.; Robb, M. A.; Cheeseman, J. R.; Scalmani, G.; Barone, V.; Petersson, G. A.; Nakatsuji et al. *Gaussian 16, Revision B.01*; Gaussian, Inc.: Wallingford CT, 2016.
- (49) Becke, A. D. Density-functional Thermochemistry. II. The Effect of the Perdew–Wang Generalized-gradient Correlation Correction. *J. Chem. Phys.* **1992**, *97*, 9173–9177.
- (50) Becke, A. D. Density-functional Thermochemistry. III. The Role of Exact Exchange. *J. Chem. Phys.* **1993**, *98*, 5648–5652.

(51) Peterson, K. A.; Puzzarini, C. Systematically Convergent Basis Sets for Transition Metals. II. Pseudopotential-Based Correlation Consistent Basis Sets for the Group 11 (Cu, Ag, Au) and 12 (Zn, Cd, Hg) Elements. *Theor. Chem. Acc.* **2005**, *114*, 283–296.

(52) Peterson, K. A. Correlation Consistent Basis Sets for Actinides. I. The Th and U Atoms. *J. Chem. Phys.* **2015**, *142*, No. 074105.

(53) Grimme, S.; Antony, J.; Ehrlich, S.; Krieg, H. A Consistent and Accurate Ab Initio Parametrization of Density Functional Dispersion Correction (DFT-D) for the 94 Elements H–Pu. *J. Chem. Phys.* **2010**, *132*, 154104.

(54) Dolg, M.; Cao, X. Accurate Relativistic Small-Core Pseudopotentials for Actinides. Energy Adjustment for Uranium and First Applications to Uranium Hydride. *J. Phys. Chem. A* **2009**, *113*, 12573–12581.

(55) Figgen, D.; Rauhut, G.; Dolg, M.; Stoll, H. Energy-Consistent Pseudopotentials for Group 11 and 12 Atoms: Adjustment to Multi-Configuration Dirac–Hartree–Fock Data. *Chem. Phys.* **2005**, *311*, 227–244.

(56) Werner, H.-J.; Knowles, P. J.; Celani, P.; Györfy, W.; Hesselmann, A.; Kats, D.; Knizia, G.; Köhn, A.; Korona, T.; Kreplin, D. et al. MOLPRO, Version 2022.0; 2022. See <https://www.molpro.net>.

(57) Werner, H.-J.; Knowles, P. J.; Knizia, G.; Manby, F. R.; Schütz, M. Molpro: A General-Purpose Quantum Chemistry Program Package. *WIREs Comput. Mol. Sci.* **2012**, *2*, 242–253.

(58) Glendening, E. D.; Landis, C. R.; Weinhold, F. NBO 7.0: New Vistas in Localized and Delocalized Chemical Bonding Theory. *J. Comput. Chem.* **2019**, *40*, 2234–2241.

(59) Bridgeman, A. J.; Cavigliasso, G.; Ireland, L. R.; Rothery, J. The Mayer Bond Order as a Tool in Inorganic Chemistry. *J. Chem. Soc., Dalton Trans.* **2001**, *14*, 2095–2108.

(60) Lu, T.; Chen, F. Multiwfn: A Multifunctional Wavefunction Analyzer. *J. Comput. Chem.* **2012**, *33*, 580–592.

(61) Huang, W.; Pal, R.; Wang, L.-M.; Zeng, X. C.; Wang, L.-S. Isomer Identification and Resolution in Small Gold Clusters. *J. Chem. Phys.* **2010**, *132*, No. 054305.

(62) Huang, W.; Wang, L.-S. Probing the 2D to 3D Structural Transition in Gold Cluster Anions Using Argon Tagging. *Phys. Rev. Lett.* **2009**, *102*, No. 153401.

(63) Stokes, S. T.; Li, X.; Grubisic, A.; Ko, Y. J.; Bowen, K. H. Intrinsic Electrophilic Properties of Nucleosides: Photoelectron Spectroscopy of Their Parent Anions. *J. Chem. Phys.* **2007**, *127*, No. 084321.

(64) Li, W.-L.; Hu, H.-S.; Jian, T.; Lopez, G. V.; Su, J.; Li, J.; Wang, L.-S. Probing the Electronic Structures of Low Oxidation-State Uranium Fluoride Molecules  $UF_x^-$  ( $x = 2-4$ ). *J. Chem. Phys.* **2013**, *139*, 244303.

(65) Su, J.; Dau, P. D.; Xu, C.-F.; Huang, D.-L.; Liu, H.-T.; Wei, F.; Wang, L.-S.; Li, J. A Joint Photoelectron Spectroscopy and Theoretical Study on the Electronic Structure of  $UCl_5^-$  and  $UCl_5$ . *Chem. – Asian J.* **2013**, *8*, 2489–2496.

(66) Persaud, R. R.; Chen, M.; Dixon, D. A. Prediction of Structures and Atomization Energies of Coinage Metals,  $(M)_n$ ,  $n < 20$ : Extrapolation of Normalized Clustering Energies to Predict the Cohesive Energy. *J. Phys. Chem. A* **2020**, *124*, 1775–1786.